

A comparative study of small x Monte Carlos with and without QCD coherence effects *

G. Chachamis¹, M. Deak², A. Sabio Vera², P. Stephens³

¹ Paul Scherrer Institut, CH-5232 Villigen PSI, Switzerland

² Instituto de Fisica Teorica UAM/CSIC, Nicolas Cabrera 15, and Universidad Autonoma de Madrid, E-28049 Madrid, Spain

³ 4800 Oak Grove Dr m/s 138-308, Pasadena 91009-8001, USA

September 10, 2020

We compare two Monte Carlo implementations of resummation schemes for the description of parton evolution at small values of Bjorken x . One of them is based on the Balitsky-Fadin-Kuraev-Lipatov (BFKL) evolution equation and generates fully differential parton distributions in momentum space making use of reggeized gluons. The other one is based on the Catani-Ciafaloni-Fiorani-Marchesini (CCFM) partonic kernel where QCD coherence effects are introduced. It has been argued that both approaches agree with each other in the $x \rightarrow 0$ limit. We show that this is not the case for azimuthal angle dependent quantities since at high energies the BFKL approach is dominated by its zero conformal spin component while the CCFM gluon Green function receives contributions from all conformal spins even at very small x .

1 Introduction

An important challenge in the phenomenology of Quantum Chromodynamics (QCD) is to understand what are the dominant effective degrees of freedom underlying the strong interaction at high energies. In the limit where the center-of-mass energy \sqrt{s} in a collision is much larger than any of the relevant mass scales the Balitsky-Fadin-Kuraev-Lipatov (BFKL) approach [1–3] appears to be a very useful framework to describe the scattering. In its original formulation this approach is based on the exchange of “reggeized” gluons in the t -channel. The interaction among them takes place via a gauge invariant (reggeized gluon)-(reggeized gluon)-(gluon) vertex. This simple effective structure stems from the dominance of the so-called multi-Regge kinematics where gluon cascades are only ordered in longitudinal components.

The simplicity of the final integral equation should not shadow the strong self-consistency of the full BFKL program where tight bootstrap conditions linking the reggeization of the gluon with the pomeron wavefunction, dominant in diffractive interactions, are fulfilled. The regime of applicability of the leading order BFKL approach to phenomenology is limited since it should be

*Preprint numbers: LPN11-04, IFT-UAM/CSIC-11-03, FTUAM-11-36

valid in a certain window of center-of-mass energies and perturbative scales. To extend its range of applicability one should include either higher order corrections, going beyond the ‘multi-Regge’ kinematics, include non-linear corrections responsible for the restauration of unitarity at very small x ¹ or, as we are going to discuss in this paper, to include a more global treatment of collinear regions in phase space using the Catani-Ciafaloni-Fiorani-Marchesini (CCFM) equation, which provides a good matching from BFKL to the $x \rightarrow 1$ regime, at least, as we are going to show in this work, as long as anomalous dimensions and k_t -diffusion properties are concerned.

In this letter we first give a brief introduction to the BFKL and CCFM approaches, in section 2. We then describe our Monte Carlo implementations in sections 3 and 4, where we also compare both resummation schemes in terms of the detailed exclusive information we can obtain from running the Monte Carlo codes. In particular, we show that the UV/IR symmetry in the k_t -diffusion present in the BFKL evolution is broken at lower energies in the CCFM equation, to then be slowly restored as x tends to 0. Our main result appears when we study the azimuthal angle dependence of the gluon Green function in both approaches. We show that the CCFM equation generates a stronger azimuthal angle dependence than the BFKL equation. To stress this point we investigate the Fourier components of the solution in this angular sector. We show that the projection on the zero Fourier component, or zero conformal spin in the BFKL context, has the highest growth with energy in both schemes. The differences appear in the non-zero Fourier components, or non-zero conformal spins, which in the BFKL description fall with energy but in the CCFM solution increase. We also discuss the different collinear behaviour of the solutions at different energies. Finally we present our conclusions and scope for further investigations.

2 Multi-Regge kinematics versus QCD coherence in small x final states

Coherence effects are already present in Quantum Electrodynamics where they are responsible for the suppression of soft bremsstrahlung from electron-positron pairs. In QCD processes such as $g \rightarrow q\bar{q}$ where a soft gluon is emitted from one of the fermionic lines with an angle larger than the angle of emission in the original $q\bar{q}$ pair probes the total colour charge of this pair. This charge is the same as that of the parent gluon and the final radiation takes place as if the soft gluon was emitted from it. This is what we call a colour coherence effect and leads to the angular ordering of sequential gluon emissions. In Deep Inelastic Scattering (DIS) we can focus on the $(i - 1)$ th emitted gluon with energy E_{i-1} from the proton. A secondary gluon radiated from it with a fraction $(1 - z_i)$ of its energy and a transverse momentum q_i has the opening angle

$$\theta_i \approx \frac{q_i}{(1 - z_i)E_{i-1}}, \quad (1)$$

with $z_i = E_i/E_{i-1}$ and $|\theta_i| \ll 1$. Colour coherence leads to angular ordering with increasing opening angles towards the hard scale, in this case the virtuality of the photon Q^2 , and we have $\theta_{i+1} > \theta_i$, or

$$\frac{q_{i+1}}{1 - z_{i+1}} > \frac{z_i q_i}{1 - z_i}, \quad (2)$$

which in the limit $z_i, z_{i+1} \ll 1$ is equivalent to $q_{i+1} > z_i q_i$.

¹In this work we consider equivalent variables the center-of-mass energy s , the DIS Bjorken x and the rapidity Y linking them by $Y \simeq \ln s \simeq \ln 1/x$.

In Refs. [4–7] the BFKL equation for the unintegrated gluon density was written in a form suitable for the study of exclusive quantities:

$$f_\omega(\mathbf{k}) = f_\omega^0(\mathbf{k}) + \bar{\alpha}_S \int \frac{d^2\mathbf{q}}{\pi q^2} \int_0^1 \frac{dz}{z} z^\omega \Delta_R(z, k) \Theta(q - \mu) f_\omega(\mathbf{q} + \mathbf{k}), \quad (3)$$

where ω is the Mellin-conjugate variable to Bjorken x , μ plays the role of a collinear cutoff, \mathbf{q} is the transverse momentum of the emitted gluon, and the reggeized gluon propagator is

$$\Delta_R(z_i, k_i) = \exp\left(-\bar{\alpha}_S \ln \frac{1}{z_i} \ln \frac{k_i^2}{\mu^2}\right), \quad (4)$$

with $k_i \equiv |\mathbf{k}_i|$, and $\bar{\alpha}_S \equiv \alpha_S N_c / \pi$. Solving the equation by iteration real gluon emissions are generated with the corresponding virtual corrections summed to all orders. Since f_ω is inclusive and IR finite it corresponds to a sum over all final states with the μ -dependence cancelling between the real and virtual contributions in the final result.

The DIS structure function is calculated integrating over all $\mu^2 \leq q_i^2 \leq Q^2$ and reads

$$F_\omega^{\text{BFKL}}(Q, \mu) \equiv \Theta(Q - \mu) + \sum_{r=1}^{\infty} \int_{\mu^2}^{Q^2} \prod_{i=1}^r \frac{d^2\mathbf{q}_i}{\pi q_i^2} dz_i \frac{\bar{\alpha}_S}{z_i} z_i^\omega \Delta_R(z_i, k_i), \quad (5)$$

where i corresponds to the number of gluon emissions, which in the leading order approximation coincides with the number of iterations of the kernel. In Ref. [5] it was pointed out that coherence effects should significantly modify each contribution to the final sum with a fixed number of emitted gluons, r , whilst preserving the sum. Therefore, care must be taken to account properly for coherence in the calculation of associated distributions.

Modifying the BFKL formalism to account for coherence [4–7], F_ω^{BFKL} becomes

$$F_\omega^{\text{CCFM}}(Q, \mu) = \Theta(Q - \mu) + \sum_{r=1}^{\infty} \int_0^{Q^2} \prod_{i=1}^r \frac{d^2\mathbf{q}_i}{\pi q_i^2} dz_i \frac{\bar{\alpha}_S}{z_i} z_i^\omega \Delta(z_i, q_i, k_i) \Theta(q_i - z_{i-1} q_{i-1}), \quad (6)$$

where $\Delta(z_i, q_i, k_i)$ is not a reggeized gluon propagator anymore but stills plays the role of a no-emission factor and takes the CCFM form

$$\Delta(z_i, q_i, k_i) = \exp\left[-\bar{\alpha}_S \ln \frac{1}{z_i} \ln \frac{k_i^2}{z_i q_i^2}\right]; \quad k_i > q_i. \quad (7)$$

For the first emission $q_0 z_0 = \mu$ is chosen. This collinear cutoff is needed only in the first emitted gluon because subsequent collinear emissions are already regulated by the angular ordering constraint.

Both approaches were compared when the rates for emission of a fixed number of resolved gluons, with a transverse momentum larger than a given resolution scale μ_R , together with any number of unresolved ones, was performed in Ref. [8]. The μ_R scale is constrained by the collinear cutoff and the hard scale, $\mu \ll \mu_R \ll Q$. It was found that jet rates in both multi-Regge (BFKL) and coherent (CCFM) schemes are the same. When coherence is introduced the singularities at $\omega = 0$ are stronger than in the BFKL approach but the extra logarithms cancel in the sum of all the contributions to the jet rates. Using a generating function for the jet multiplicity it is possible to prove that this is true to all orders in the coupling [9, 10]. The same generating function is obtained

for BFKL and CCFM, with the p -th central moment of the jet multiplicity distribution being a polynomial in $\frac{\bar{\alpha}_s}{\omega} \ln \frac{Q}{\mu_R}$ of degree $2p - 1$, showing that the distribution becomes relatively narrow in the limit of very small x and large Q/μ_R [9].

In Refs. [11] the subject was developed further and subleading logarithms were included to calculate the minijet multiplicity associated to Higgs production at hadron colliders. In [12] it was also shown that for any sufficiently inclusive observable the CCFM formalism should lead to the same results as the BFKL equation. For the interested reader good reviews devoted to the implementation of CCFM in Monte Carlo event generators can be found in, *e.g.*, [14–17]. For Monte Carlo implementations of the BFKL approach see Refs. [13–16, 18–22]. More recent results related to the implementation of models with unitarization in the CCFM formalism can be found in Refs. [23, 24]

3 Monte Carlo implementation of the CCFM evolution and numerical results

The numerical implementation of the CCFM equation we use in the present work is the Monte Carlo event generator **SMALLX** developed by Marchesini and Webber in Ref. [25]. In this code the CCFM gluon Green function, interpreted as the unintegrated gluon structure function $f^{\text{CCFM}}(\mathbf{k}_a, \mathbf{k}_b, x)$ when acting on the initial condition shown below, can be written in the iterative form

$$f^{\text{CCFM}}(\mathbf{k}_a, \mathbf{k}_b, x) = \delta(x - x_0) \delta^{(2)}(\mathbf{k}_a - \mathbf{k}_b) \Delta_S(\eta, q_0) \theta(\eta - q_0) + \sum_{n=1}^{\infty} \int \left[\prod_{i=1}^n d\text{PS}_i \right] \theta(\eta - z_n l_n) \Delta_S(\eta, z_n l_n) \delta(x - x_n) \delta^{(2)}(\mathbf{k}_a - \mathbf{k}_n). \quad (8)$$

As we mentioned in the previous section, q_0 is the collinear cutoff for the first real emission. \mathbf{k}_i corresponds to the transverse momentum of the exchanged gluons, with x_i being their longitudinal momentum fraction. $l_i = q_i/(1 - z_i)$ is the rescaled transverse momentum of the emitted gluons. η is the upper limit of the phase space integration. The Sudakov form factor reads

$$\Delta_S(l_i, z_{i-1} l_{i-1}) = \exp \left[-2\bar{\alpha}_s \int_{z_{i-1} l_{i-1}}^{l_i} \frac{dl}{l} \int_0^{1-\frac{\lambda}{l}} \frac{dz}{1-z} \right], \quad (9)$$

where λ is a cutoff for soft singularities. The final result is independent of λ in the limit $\lambda \rightarrow 0$. The probability of emission of each of the real gluons can be written in the form

$$d\text{PS}_i = \Delta_S(l_i, z_{i-1} l_{i-1}) P(z_i, q_i, k_i) \theta(l_i - z_{i-1} l_{i-1}) \theta \left(1 - z_i - \frac{\lambda}{l_i} \right) \frac{d^2 \mathbf{l}_i}{\pi l_i^2} dz_i, \quad (10)$$

with the gluon splitting function being

$$P(z_i, q_i, k_i) = \bar{\alpha}_s \left(\frac{1}{1 - z_i} + \frac{\Delta(z_i, q_i, k_i)}{z_i} \right). \quad (11)$$

Our target is to compare this numerical implementation of the solution to the CCFM equation with the corresponding one in the BFKL approach. For this we have studied several distinctive distributions which will allow for the comparison. In this letter we focus on the leading order approximation in both approaches keeping the coupling fixed. We will investigate higher order corrections in future publications.

If we represent the CCFM solution in the iterative form of Eq. (8) we can test its convergence investigating what is the contribution to f^{CCFM} stemming from a fixed number of real gluon emissions. For a given $x = e^{-Y}$ when Y is larger configurations with more emissions have a bigger weight. This is seen in Fig. 1 where we also notice that the maximum of the distribution, with $\bar{\alpha}_s = 0.2$, for $Y = 2, 4, 6, 8$ lies, respectively, at $n = 4, 5, 7, 9$. The chosen external momentum

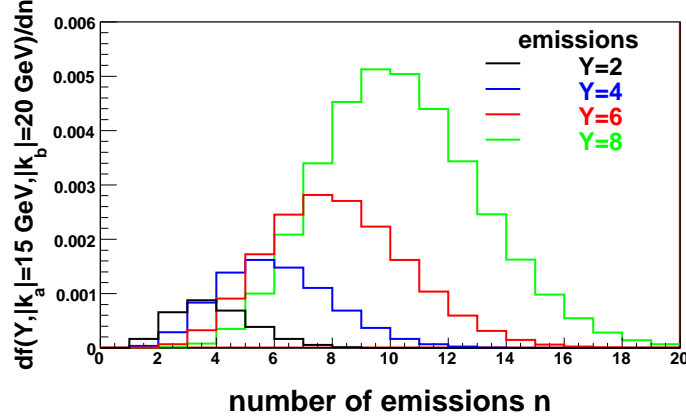


Figure 1: Distribution in the contributions to the CCFM gluon Green function with a fixed number of emitted gluons, plotted for different values of the center-of-mass energy.

scales are $k_a = 15, k_b = 20$ GeV. In Fig. 2 we observe that the shape of the distribution is better reproduced by a Gaussian than by a Poissonian fit.

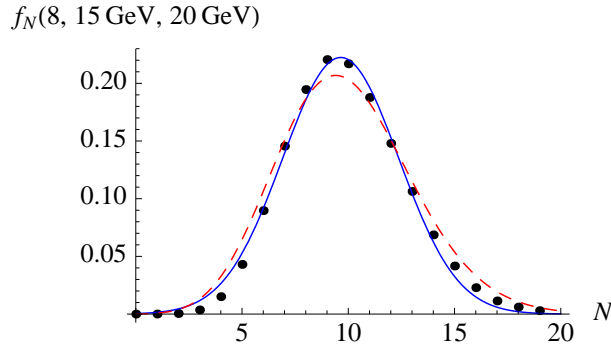


Figure 2: Gaussian (straight) and Poissonian (dashed) fits to the distribution in the contributions to the CCFM gluon Green function with a fixed number of emitted gluons, plotted for rapidity $Y = 8$ and fixed values of the external momenta.

As the gluon emissions take place it is more likely to populate regions of phase space far away from the transverse scales present in the initial condition. We have studied this point in Fig. 3 where we show the mean deviation from the central value of the typical transverse momentum of the emitted gluons from the external scales k_a, k_b . We continue choosing $\bar{\alpha}_s = 0.2$ and we now take $k_a = 15$ GeV and $k_b = 20$ GeV. The central lines show the maximum of the distribution in the momentum of the emitted gluon k for a given rapidity Y , showing all plots with different total

rapidities in a single figure normalizing them to the interval from zero to one. The two outermost lines correspond to $Y = 8$ with the total Y decreasing as we move closer to the central line. It is

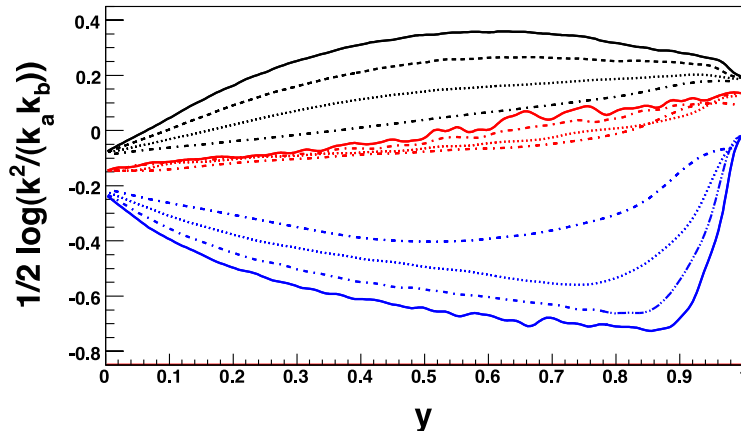


Figure 3: Distribution of transverse scales in the evolution with x of the CCFM equation.

very interesting to see how the diffusion into the infrared region, where $k^2 < k_a k_b$, dominates the evolution. To quantify this statement we have calculated the ratio

$$\mathcal{R}_{\text{UV/IR}} = \frac{\text{Area}_{\text{UV}}}{\text{Area}_{\text{IR}}} \quad (12)$$

of the area above (ultraviolet diffusion) over the area below (infrared diffusion) the central line. For $Y = 2, 4, 6, 8$ we obtain $\mathcal{R}_{\text{UV/IR}} = 0.42, 0.43, 0.44, 0.47$. From these numbers we can see that the contribution of the infrared region is enhanced as we decrease the available energy in the scattering process. If we introduce a cut in the number of gluons considering only those contributions to the gluon Green function with more than 10 emissions then we obtain $\mathcal{R}_{\text{UV/IR}} = 0.39, 0.48, 0.51$ for, respectively, $Y = 4, 6, 8$. This indicates that high-multiplicity contributions are more dominated by infrared effects for low total rapidities than the low-multiplicity configurations, while converging to a more UV/IR symmetric structure for larger Y . This is natural since they dominate the full Green function in this region.

When comparing with the BFKL results, it is interesting to investigate the collinear/anticollinear behaviour of the solution to the CCFM equation. This can be done by studying, with a fixed rapidity Y , the regions with large/small ratio of the external scales k_b/k_a . We have done this in Fig. 4 for different values of the ‘reference scale’ $k_b = 5, 10, 30$ GeV. The main conclusion of this analysis is that at lower values of the external scale k_b the gluon Green function becomes much flatter as a function of the variation of the other external scale k_a . One is naturally tempted to relate this behaviour to a possible approximate ‘conformal invariance’ present in this limit. If we now introduce a cut in the number of emissions and keep only those contributions with more than ten gluons in the final state then we obtain Fig. 5. We can see that the approximate scale invariance present in the low k_b cases remains in the low-multiplicity configurations, being a quite universal feature of the CCFM radiation.

We now focus on the azimuthal angle dependence of our numerical solution. The azimuthal angle, θ , we are interested in is that formed by the two two-dimensional external vectors \mathbf{k}_a and \mathbf{k}_b .

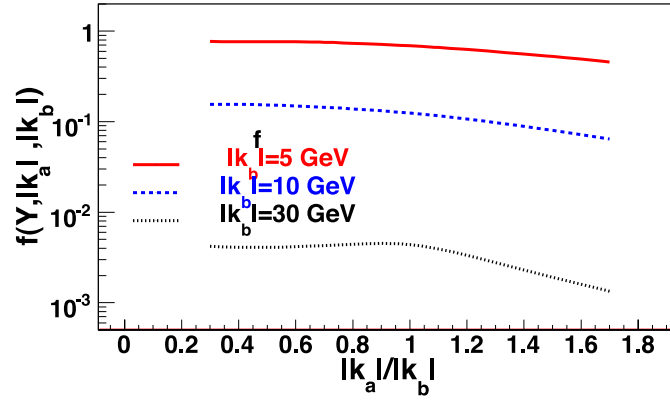


Figure 4: Collinear behaviour of the CCFM gluon Green function for different values of the reference scale, k_b .

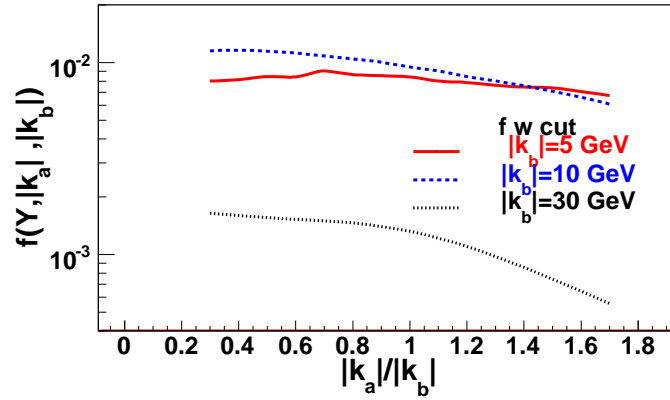


Figure 5: Collinear behaviour of the CCFM gluon Green function for different values of the reference scale, k_b , considering the contributions of configurations with more than 10 emissions.

For this we extract the corresponding Fourier components using

$$f_n^{\text{CCFM}}(k_a, k_b, x) = \int_0^{2\pi} \frac{d\theta}{2\pi} f^{\text{CCFM}}(\mathbf{k}_a, \mathbf{k}_b, x) \cos(n\theta). \quad (13)$$

In Fig. 6 we observe that the $n = 0$ component is the dominant one, with the $n > 0$ components also growing with energy but at a slower pace. We will see that this is completely different to the BFKL case. If we impose the high-multiplicity cut then we can see in Fig. 7 that at larger Y the Green function is completely dominated by the many-gluon configurations. We can also conclude that the growth of all Fourier components is a common feature at any multiplicity.

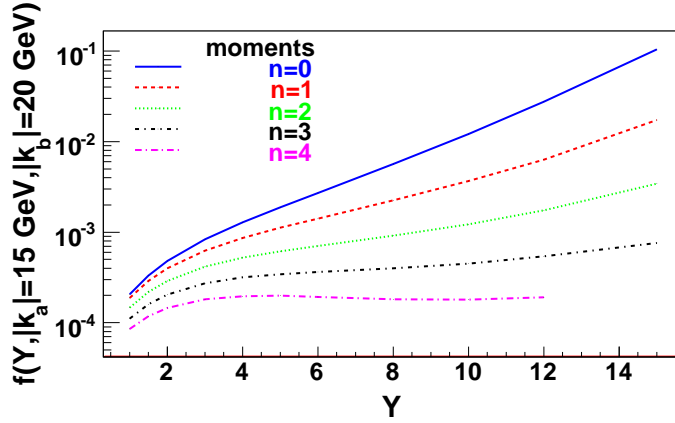


Figure 6: Variation with rapidity of the different components of the Fourier expansion on the azimuthal angle of the CCFM gluon Green function.

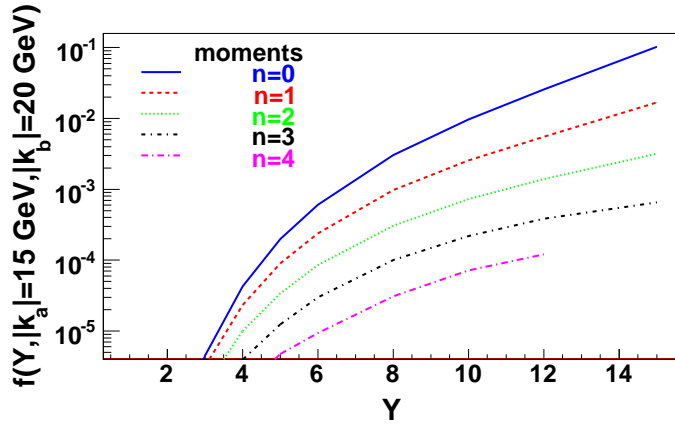


Figure 7: Variation with rapidity of the different components of the Fourier expansion on the azimuthal angle of the CCFM gluon Green function, considering the contributions of configurations with more than 10 emissions.

To wrap up this section we consider the full θ dependence in Fig. 8. It is clear that the bulk of the configurations live in the region with \mathbf{k}_a “back-to-back” with \mathbf{k}_b ($\theta = 0$) with a Gaussian-like spread towards other angular settings. At high multiplicities the \mathbf{k}_a and \mathbf{k}_b momenta tend to be more

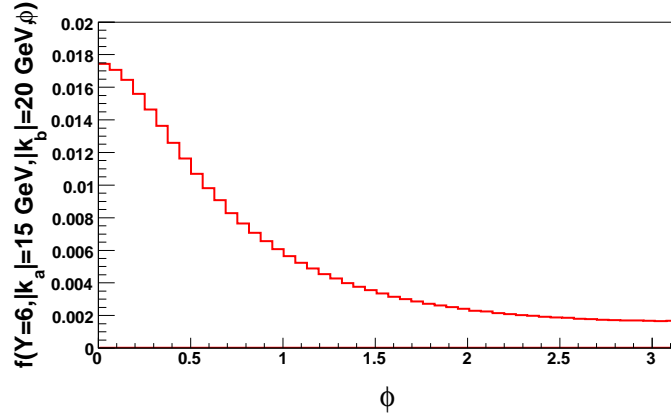


Figure 8: Full dependence on the azimuthal angle of the CCFM gluon Green function.

decorrelated in the azimuthal angle as seen in Fig. 9. The combined (θ, Y) dependence is shown

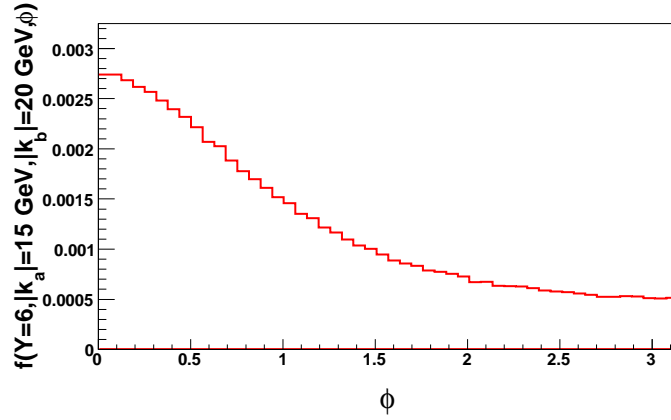


Figure 9: Full dependence on the azimuthal angle of the CCFM gluon Green function, considering the contributions of configurations with more than 10 emissions.

in Fig. 10. When only the high-multiplicity configurations are kept we obtain a slower variation in angles in Fig. 11.

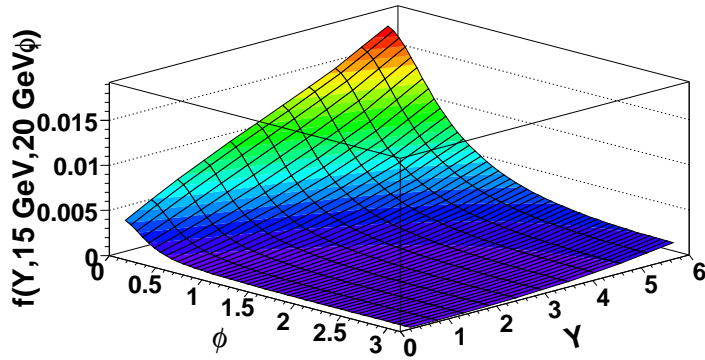


Figure 10: The combined dependence of the CCFM gluon Green function on the azimuthal angle and rapidity, for fixed values of the modulus of the boundary momenta.

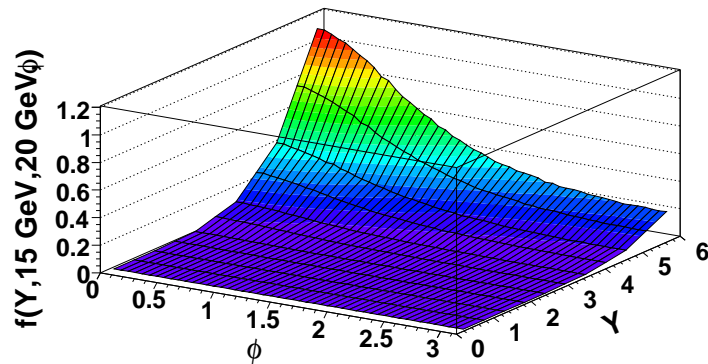


Figure 11: The combined dependence of the CCFM gluon Green function on the azimuthal angle and rapidity, for fixed values of the modulus of the boundary momenta, considering the contributions of configurations with more than 10 emissions.

4 Monte Carlo implementation of the BFKL evolution and numerical results

Our numerical solution of the BFKL equation is based on the following iterative representation for the LO gluon Green function:

$$f^{\text{BFKL}}(\mathbf{k}_a, \mathbf{k}_b, Y) = e^{2\omega_0(-k_a^2)Y} \left\{ \delta^{(2)}(\mathbf{k}_a - \mathbf{k}_b) + \sum_{n=1}^{\infty} \prod_{i=1}^n \bar{\alpha}_s \int \frac{d^2\mathbf{k}_i}{\pi k_i^2} \theta(k_i^2 - \lambda^2) \int_0^{y_i} dy_i e^{2\omega_0^{(i,i-1)}y_i} \delta^{(2)}\left(\mathbf{k}_a - \mathbf{k}_b + \sum_{l=1}^n \mathbf{k}_l\right) \right\}, \quad (14)$$

where

$$\omega_0^{(i,i-1)} \equiv \omega_0\left(-\left(\mathbf{k}_1 + \sum_{l=1}^i \mathbf{k}_l\right)^2\right) - \omega_0\left(-\left(\mathbf{k}_1 + \sum_{l=1}^{i-1} \mathbf{k}_l\right)^2\right). \quad (15)$$

Here we have used this notation for the gluon Regge trajectory:

$$\omega_0(t) = -\frac{\bar{\alpha}_s q^2}{4\pi} \int \frac{d^2\mathbf{k}}{k^2(\mathbf{q} - \mathbf{k})^2} \simeq -\frac{\bar{\alpha}_s}{2} \log \frac{q^2}{\lambda^2}, \quad (16)$$

where $t = -q^2$ and λ is an infrared regulator. The final result is independent of λ in the limit of small λ . The normalization of our numerical implementation corresponds to the following analytic form of the Green function:

$$f^{\text{BFKL}}(\mathbf{k}_a, \mathbf{k}_b, Y) = \frac{1}{\pi k_a k_b} \sum_{n=-\infty}^{\infty} \int \frac{d\omega}{2\pi i} e^{\omega Y} \int \frac{d\gamma}{2\pi i} \left(\frac{k_a^2}{k_b^2}\right)^{\gamma - \frac{1}{2}} \frac{e^{in\theta}}{\omega - \bar{\alpha}_s \chi(n, \gamma)}, \quad (17)$$

where θ is the azimuthal angle between the \mathbf{k}_a and \mathbf{k}_b transverse momenta. In the case of elastic scattering n can be interpreted as a conformal spin in the unitary principal series representation of $SL(2, C)$ [26]. The eigenvalue of the BFKL kernel is

$$\chi(n, \gamma) = 2\Psi(1) - \Psi\left(\gamma + \frac{n}{2}\right) - \Psi\left(1 - \gamma + \frac{n}{2}\right). \quad (18)$$

The Monte Carlo analysis is useful because it allows for a more detailed study of different distributions. In particular, we can, as we did in the CCFM case, investigate the convergence of the iterative solution in terms of the contributions with a fixed number of emissions for a given value of $Y \simeq \log 1/x$. We have shown this distribution in Fig. 12 for $Y = 2, 4, 6, 8$, $k_a = 15$ GeV and $k_b = 20$ GeV and $\bar{\alpha}_s = 0.2$. We observe a very similar pattern to the one present in the CCFM case: a broadening towards larger number of emissions for large rapidities with the maxima being at $n = 2, 5, 8, 11$ for, respectively, $Y = 2, 4, 6, 8$. The main difference here is that in the BFKL case the distribution is clearly Poissonian.

The diffusion picture in BFKL at leading order is well understood. We can average over the azimuthal angle:

$$\begin{aligned} \bar{f}^{\text{BFKL}}(k_a, k_b, Y) &\equiv \frac{1}{2\pi} \int_0^{2\pi} f^{\text{BFKL}}(\mathbf{k}_a, \mathbf{k}_b, Y) \\ &= \frac{1}{\pi k_a k_b} \int \frac{d\omega}{2\pi i} \int \frac{d\gamma}{2\pi i} \left(\frac{k_a^2}{k_b^2}\right)^{\gamma - \frac{1}{2}} \frac{e^{\omega Y}}{\omega - \bar{\alpha}_s \chi(\gamma)}, \end{aligned} \quad (19)$$

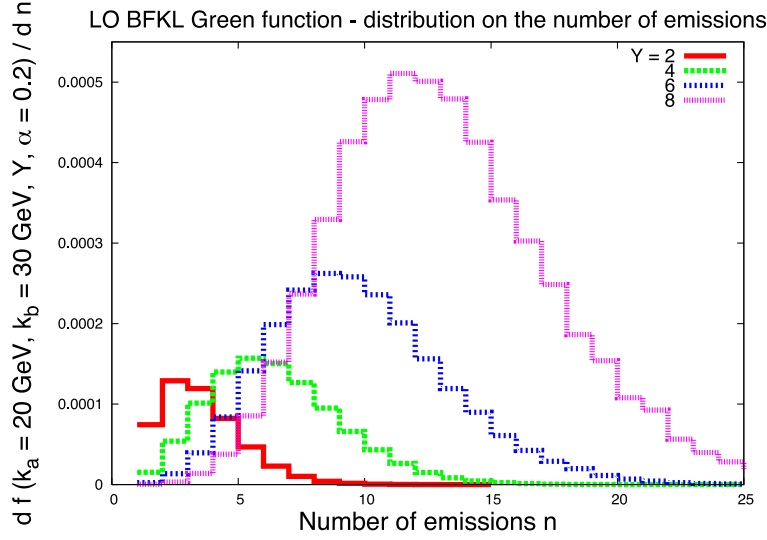


Figure 12: Distribution in the contributions to the BFKL gluon Green function with a fixed number of emitted gluons, plotted for different values of the center-of-mass energy.

where $\chi(\gamma)$ has poles at integer values of γ with the physical region corresponding to $0 < \gamma < 1$. At asymptotic values of Y the dominant region of integration corresponds to $\gamma \simeq \frac{1}{2}$. The $\gamma \leftrightarrow 1 - \gamma$ symmetry of χ indicates that there exists a symmetric diffusion into infrared and ultraviolet modes: since the pole at $\gamma \simeq 0$ (1) corresponds to virtualities in the internal propagators smaller (larger) than the external scales, it leads to infrared (ultraviolet) diffusion. To be more precise: for very large values of $\bar{\alpha}_s Y$ we can write

$$\bar{f}^{\text{BFKL}}(k_a, k_b, Y) = \frac{1}{\pi k_a k_b} \int \frac{d\gamma}{2\pi i} \left(\frac{k_a^2}{k_b^2} \right)^{\gamma - \frac{1}{2}} e^{\chi(\gamma) \bar{\alpha}_s Y}, \quad (20)$$

and evaluate the integral using the saddle point approximation around the minimum of χ :

$$\chi(\gamma) \simeq 4 \log 2 + 14 \zeta_3 \left(\gamma - \frac{1}{2} \right)^2 + \dots \quad (21)$$

to obtain the expression

$$\bar{f}^{\text{BFKL}}(k_a, k_b, Y) \simeq \frac{1}{2\pi k_a k_b} e^{\bar{\alpha}_s 4 \log 2 Y} \frac{1}{\sqrt{14\pi \zeta_3 \bar{\alpha}_s Y}} e^{\frac{-t^2}{56\zeta_3 \bar{\alpha}_s Y}}, \quad (22)$$

with $t \equiv \log(k_a^2/k_b^2)$. It is easy to verify that the function

$$\Phi(k_a, k_b, Y) \equiv k_a k_b \bar{f}^{\text{BFKL}}(k_a, k_b, Y) \quad (23)$$

asymptotically fulfills the diffusion equation

$$\frac{\partial \Phi}{\partial (\bar{\alpha}_s Y)} = 4 \log 2 \Phi + 14 \zeta_3 \frac{\partial^2 \Phi}{\partial t^2}, \quad (24)$$

which is independent of the sign of t and therefore, going back to the definition in Eq. (12), $\mathcal{R}_{UV/IR} = 1$ in the BFKL case. It is interesting to note that this diffusive behaviour is only driven by the anomalous dimension γ while the $n \neq 0$ do not play any role. The fact that in the CCFM case the ratio $\mathcal{R}_{UV/IR}$ tends to 1 for very large rapidities is in agreement with the fact in the small x limit the CCFM and BFKL approaches have the same asymptotic limit for the anomalous dimensions governing the scale variation of DIS structure functions.

The collinear/antcollinear limits, at leading order, are not as interesting as in the CCFM case since the Green function has the functional form $g(k_a/k_b)/(k_a k_b)$. Changing the reference scale k_b does not bring any new features as we can see in Fig. 13, where we chose $Y = 6$. When imposing a cut to only keep high-multiplicity contributions we obtain a similar result, see Fig. 14

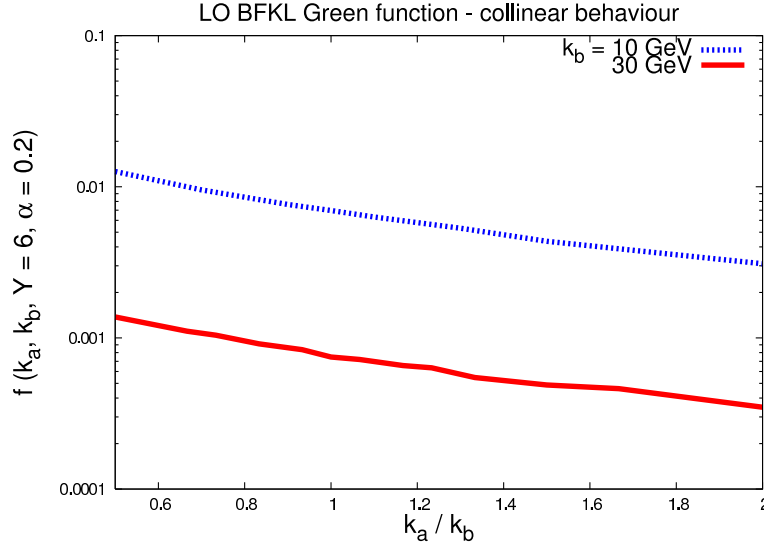


Figure 13: Collinear behaviour of the BFKL gluon Green function for different values of the reference scale k_a

Apart from the different diffusive behaviour, it is in the azimuthal angle dependence where we find more differences between the BFKL and the CCFM approaches. The expansion on Fourier components in the azimuthal angle can be written as

$$f^{\text{BFKL}}(\mathbf{k}_a, \mathbf{k}_b, Y) = \sum_{n=-\infty}^{\infty} f_n^{\text{BFKL}}(k_a, k_b, Y) e^{in\theta}, \quad (25)$$

with the coefficients being

$$f_n^{\text{BFKL}}(k_a, k_b, Y) = \frac{1}{\pi k_a k_b} \int \frac{d\gamma}{2\pi i} \left(\frac{k_a^2}{k_b^2} \right)^{\gamma - \frac{1}{2}} e^{\alpha \chi_n(\gamma) Y}. \quad (26)$$

When performing our Monte Carlo analysis we obtain these coefficients using the momentum space numerical solution projecting on angles, i.e.

$$f_n^{\text{BFKL}}(k_a, k_b, Y) = \int_0^{2\pi} \frac{d\theta}{2\pi} f^{\text{BFKL}}(\mathbf{k}_a, \mathbf{k}_b, Y) \cos(n\theta). \quad (27)$$

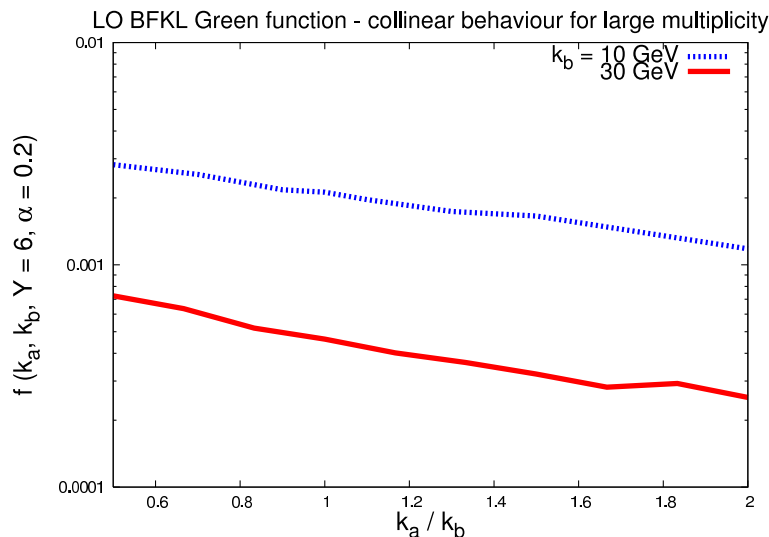


Figure 14: Collinear behaviour of the BFKL gluon Green function for different values of the reference scale k_a , considering the contributions of configurations with more than 10 emissions.

In Fig. 15 we show how the convergence in n for the Green function is very fast. In this example we can see that 10 terms in the series are enough to reach a very good approximation to the final solution. This agrees with the general behaviour obtained with our Monte Carlo analysis in Fig. 16. The combined plots in rapidity and azimuthal angle for full and high multiplicities are given in Fig. 17 and Fig. 18.

Very importantly, in the BFKL approach the Fourier projections in θ have a very different behaviour to those in the CCFM formalism. As we can observe in Fig. 19 the $n = 0$ projection also rises as in the CCFM case in Fig. 6. However, the non-zero n BFKL components do not rise with Y while the CCFM ones do rise, see, again, Fig. 6. This indicates that any observable sensitive to these higher angular components will have a completely different behaviour in both theories. There has been recent progress in the study of the azimuthal angle dependence within the BFKL approach, see, *e.g.*, Refs. [27–31, 36–38]. In future publications we will present observables where this different azimuthal angle dependence might help discriminate between BFKL and CCFM contributions. A natural candidate is the azimuthal angle decorrelation between jets produced in the central region of rapidity and a jet emitted along the direction of one of the hadrons in the Large Hadron Collider.

5 Conclusions and scope

In this letter we have compared two Monte Carlo implementations of the CCFM and BFKL formalisms for the description of small x observables. The main difference between them from the theoretical point of view is the introduction of QCD coherence effects in the CCFM equation. We have found that the symmetric diffusion into infrared and ultraviolet regions of phase space characteristic of the BFKL parton evolution is broken in the CCFM case, where the infrared scales play a dominant role. As our main result we have found that the higher Fourier components in the gluon Green function have a very different behaviour in both theories, rising with energy in the CCFM case and decreasing in the BFKL one. It will be very interesting to trace these

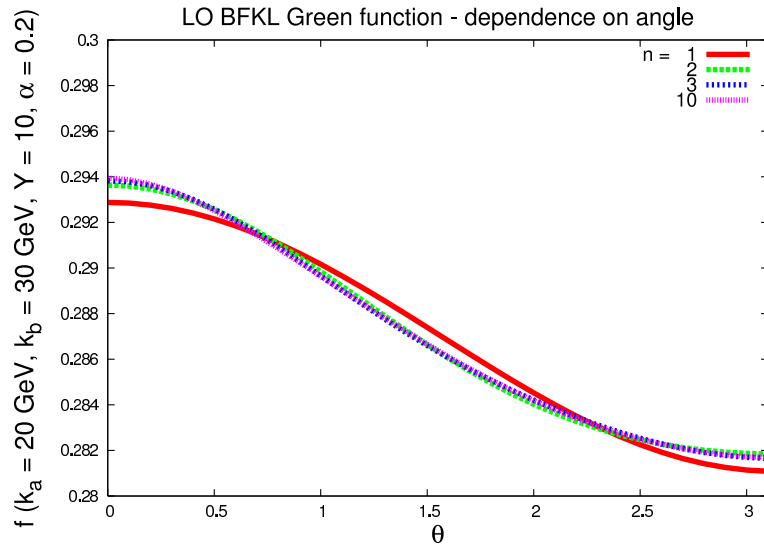


Figure 15: Azimuthal angle dependence of the BFKL Green function. We plot the result for the sum in Eq. (25) with up to $n = 1, 2, 3, 10$ terms.

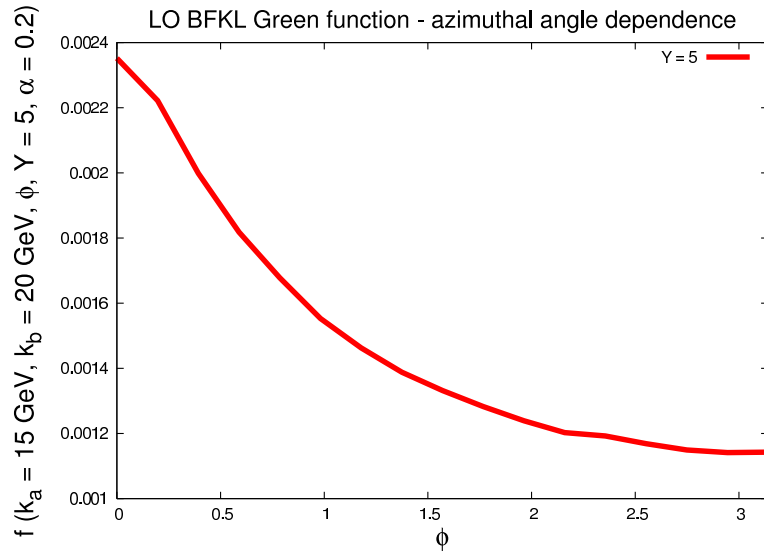


Figure 16: Full dependence on the azimuthal angle of the BFKL gluon Green function.

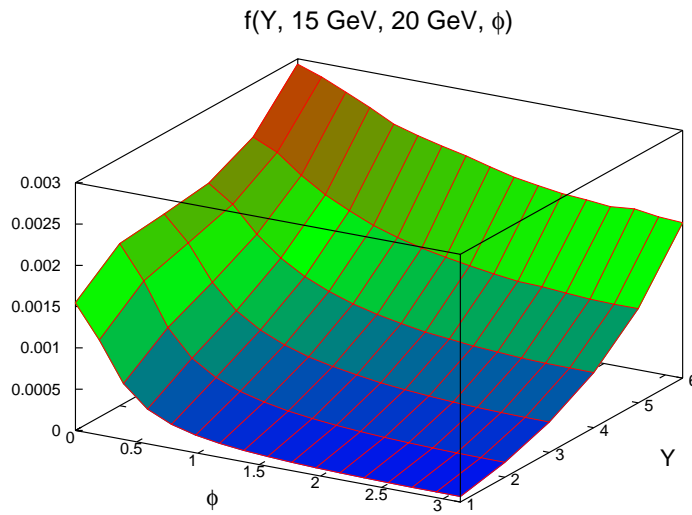


Figure 17: The combined dependence of the BFKL gluon Green function on the azimuthal angle and rapidity, for fixed values of the modulus of the boundary momenta.

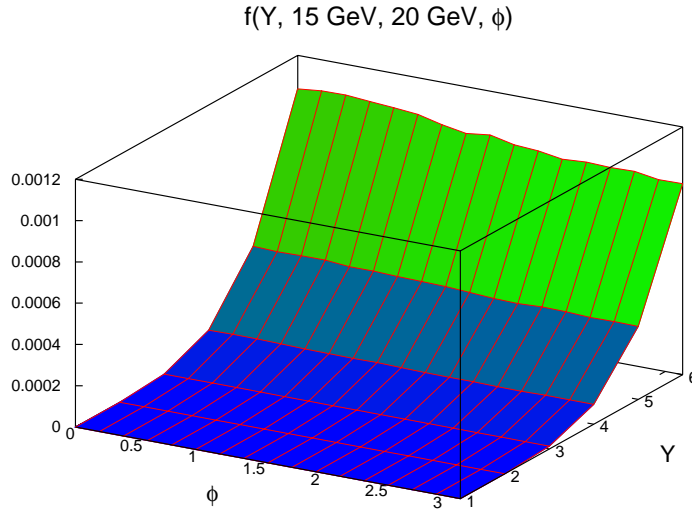


Figure 18: The combined dependence of the BFKL gluon Green function on the azimuthal angle and rapidity, for fixed values of the modulus of the boundary momenta, considering the contributions of configurations with more than 10 emissions.

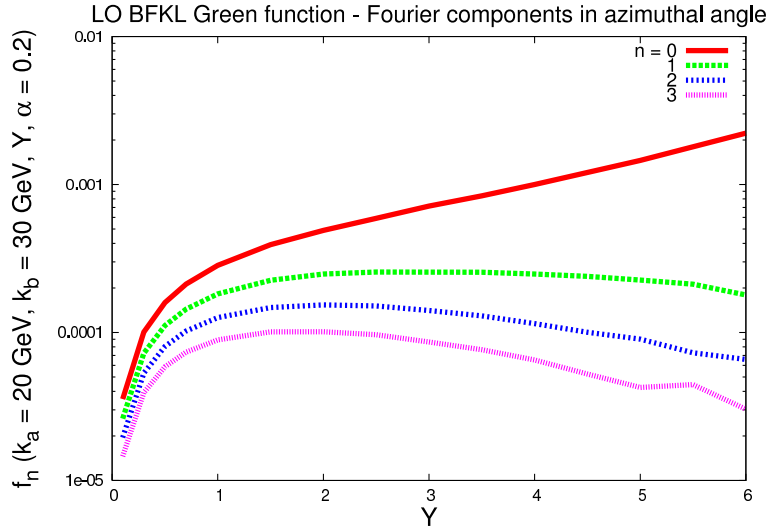


Figure 19: Variation with rapidity of the different components of the Fourier expansion on the azimuthal angle of the BFKL gluon Green function.

differences at an observable level [32–35] and to implement higher order corrections [36, 39–47] to evaluate their effects on them. These lines of research will be the subject of our future investigations.

Acknowledgements

This work has been partially supported by the European Commission under contract LHCPhenoNet (PITN-GA-2010-264564) and the Comunidad de Madrid through Proyecto HEPHACOS ESP-1473. M. D. acknowledges the support of the European Union through the Marie Curie Research Training Network “UniverseNet” (MRTCN-CT-2006-035863).

References

- [1] L. N. Lipatov, *Sov. J. Nucl. Phys.* **23** (1976) 338.
- [2] E. A. Kuraev, L. N. Lipatov, V. S. Fadin, *Phys. Lett. B* **60** (1975) 50, *Sov. Phys. JETP* **44** (1976) 443, *Sov. Phys. JETP* **45** (1977) 199.
- [3] I. I. Balitsky, L. N. Lipatov, *Sov. J. Nucl. Phys.* **28** (1978) 822.
- [4] S. Catani, F. Fiorani and G. Marchesini, *Phys. Lett.* **B234**, 339 (1990).
- [5] G. Marchesini, *Nucl. Phys.* **B445**, 49 (1995).
- [6] M. Ciafaloni, *Nucl. Phys.* **B296**, 49 (1988).
- [7] S. Catani, F. Fiorani, G. Marchesini and G. Oriani, *Nucl. Phys.* **B361**, 645 (1991).
- [8] J. R. Forshaw and A. Sabio Vera, *Phys. Lett.* **B440** (1998) 141.

- [9] B. R. Webber, Phys. Lett. **B444** (1998) 81.
- [10] J. R. Forshaw, A. Sabio Vera and B. R. Webber, J. Phys. G **G25** (1999) 1511.
- [11] C. Ewerz and B. R. Webber, JHEP **9904** (1999) 022, JHEP **9908** (1999) 019.
- [12] G. P. Salam, JHEP **9903** (1999) 009.
- [13] C. R. Schmidt, Phys. Rev. Lett. **78** (1997) 4531-4535. [hep-ph/9612454].
- [14] M. Dittmar *et al.*, arXiv:hep-ph/0511119.
- [15] S. Alekhin *et al.*, arXiv:hep-ph/0601012, arXiv:hep-ph/0601013.
- [16] J. R. Andersen *et al.* [Small x Collaboration], Eur. Phys. J. C **48** (2006) 53.
- [17] H. Jung, S. Baranov, M. Deak *et al.*, Eur. Phys. J. **C70** (2010) 1237-1249. [arXiv:1008.0152 [hep-ph]].
- [18] J. R. Andersen and A. Sabio Vera, Phys. Lett. B **567** (2003) 116, Nucl. Phys. B **679** (2004) 345. Nucl. Phys. B **699** (2004) 90, JHEP **0501** (2005) 045.
- [19] M. Dobbs *et al.*, arXiv:hep-ph/0403100.
- [20] A. Sabio Vera, arXiv:hep-ph/0307046, arXiv:hep-ph/0408008, arXiv:hep-ph/0510046.
- [21] A. Sabio Vera and P. Stephens, PoS D **IFF2006** (2006) 030.
- [22] H. Jung *et al.*, arXiv:0809.0549 [hep-ph].
- [23] E. Avsar and E. Iancu, Nucl. Phys. A **829** (2009) 31.
- [24] E. Avsar and A. M. Stasto, JHEP **1006** (2010) 112.
- [25] G. Marchesini and B. R. Webber, Nucl. Phys. B **349** (1991) 617, Nucl. Phys. B **386** (1992) 215.
- [26] L. N. Lipatov, Sov. Phys. JETP **63** (1986) 904-912.
- [27] J. Kwiecinski, A. D. Martin, L. Motyka *et al.*, Phys. Lett. **B514** (2001) 355-360. [hep-ph/0105039].
- [28] C. Marquet, C. Royon, Phys. Rev. **D79** (2009) 034028. [arXiv:0704.3409 [hep-ph]].
- [29] D. Colferai, F. Schwennsen, L. Szymanowski *et al.*, JHEP **1012** (2010) 026. [arXiv:1002.1365 [hep-ph]].
- [30] A. Sabio Vera, Nucl. Phys. B **746** (2006) 1.
- [31] A. Sabio Vera and F. Schwennsen, Nucl. Phys. B **776** (2007) 170, Phys. Rev. D **77** (2008) 014001, arXiv:hep-ph/0611151, arXiv:0707.0256 [hep-ph], arXiv:0710.1478 [hep-ph].
- [32] M. Deak, F. Schwennsen, JHEP **0809** (2008) 035. [arXiv:0805.3763 [hep-ph]].
- [33] M. Deak, F. Hautmann, H. Jung *et al.*, JHEP **0909** (2009) 121. [arXiv:0908.0538 [hep-ph]].
- [34] M. Deak, A. Grebenyuk, F. Hautmann *et al.*, [arXiv:1006.5401 [hep-ph]].

- [35] M. Deak, F. Hautmann, H. Jung *et al.*, [arXiv:1012.6037 [hep-ph]].
- [36] A. Sabio Vera, Acta Phys. Polon. B **39** (2008) 2213 [arXiv:0803.4485 [hep-ph]].
- [37] G. Chachamis, M. Hentschinski, A. Sabio Vera and C. Salas, arXiv:0911.2662 [hep-ph].
- [38] S. Baranov *et al.*,
- [39] V. S. Fadin and L. N. Lipatov, Phys. Lett. B **429** (1998) 127.
- [40] M. Ciafaloni and G. Camici, Phys. Lett. B **430** (1998) 349.
- [41] G. P. Salam, JHEP **9807**, 019 (1998).
- [42] A. Sabio Vera, Nucl. Phys. B **722** (2005) 65.
- [43] C. R. Schmidt, Phys. Rev. D **60** (1999) 074003.
- [44] J. R. Forshaw, D. A. Ross and A. Sabio Vera, Phys. Lett. B **455** (1999) 273, Phys. Lett. B **498** (2001) 149,
- [45] G. Chachamis, M. Lublinsky and A. Sabio Vera, Nucl. Phys. A **748** (2005) 649.
- [46] J. Bartels, A. Sabio Vera and F. Schwennsen, JHEP **0611** (2006) 051, PoS D **IFF2006** (2006) 029, arXiv:0709.3249 [hep-ph].
- [47] F. Caporale, A. Papa and A. Sabio Vera, Eur. Phys. J. C **53** (2008) 525, Acta Phys. Polon. B **39** (2008) 2571.